J. Marine Sci. Appl. (2013) 12: 473-483
DOI: 10.1007/s11804-013-1219-5

Energy Analysis of a Combined Solid Oxide Fuel Cell with a Steam Turbine Power Plant for Marine Applications

Yousri M. A. Welaya*, M. Mosleh and Nader R. Ammar

Department of Naval Architecture & Marine Engineering, Alexandria University, Alexandria, Egypt

Abstract: Strong restrictions on emissions from marine power plants (particularly SO_x, NO_x) will probably be adopted in the near future. In this paper, a combined solid oxide fuel cell (SOFC) and steam turbine fuelled by natural gas is proposed as an attractive option to limit the environmental impact of the marine sector. The analyzed variant of the combined cycle includes a SOFC operated with natural gas fuel and a steam turbine with a single-pressure waste heat boiler. The calculations were performed for two types of tubular and planar SOFCs, each with an output power of 18 MW. This paper includes a detailed energy analysis of the combined system. Mass and energy balances are performed not only for the whole plant but also for each component in order to evaluate the thermal efficiency of the combined cycle. In addition, the effects of using natural gas as a fuel on the fuel cell voltage and performance are investigated. It has been found that a high overall efficiency approaching 60% may be achieved with an optimum configuration using the SOFC system. The hybrid system would also reduce emissions, fuel consumption, and improve the total system efficiency.

Keywords: marine steam turbine; natural gas fuel; solid oxide fuel cell; hybrid system; energy analysis

Article ID: 1671-9433(2013)04-0473-12

1 Introduction

1.1 Emissions from ships

Ships are responsible for 15% of global NO_x emissions, 6% of global sulphur emissions and 2% of CO_2 emissions from fossil fuels. In addition, they are accountable for some 5%-10 % of acid rain amounts in coastal regions (James, 2007; Figari *et al*., 2011). Both national authorities and international organizations have developed manya large number of restrictive regulations to reduce emissions from ships. Now the rate of emissions is an important factor in the to consider selection of for power plants to that cope with the international requirements.

The International Maritime Organization (IMO) has included greenhouse gas (GHG) emission reduction in its agenda since 1995. The IMO has adopted two different emission indexes for a vessel: the Energy Efficiency Design Index (EEDI) and the Energy Efficiency Operational Indicator (EEOI). Both indexes represent the ratio between emissions, in mass of CO_2, and the transported cargo quantity per sailed distance. Regulations were adopted as an amendment to the MARPOL Annex VI in October 2010 (Figari *et al.*, 2011).

The IMO requirements for maximum sulphur content in any fuel used onboard ships changed from 4.5% to 3.5% as from in January 2012. Also, from beginning in January 2020 sulphur content should will not be allowed to not exceed 0.5% (Greensmith, 2010).

In addition, the IMO has issued regulations limiting NO_x levels from for marine diesel engines as shown in Fig. 1. These regulations include: Tier I for ships constructed from between Jan. 2000 to and Dec. 2010, Tier II for ships constructed from between Jan. 2011 to and Dec. 2015, and Tier III for ships constructed from Jan. 2016 onwards when located in a NO_x emission control area (ECA) (Greensmith, 2010).

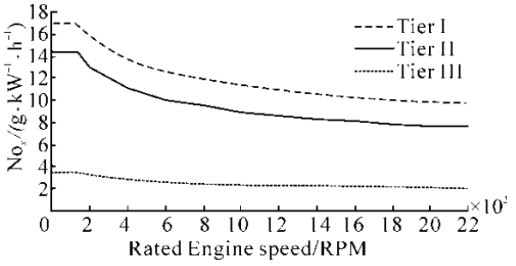

Fig. 1 Maximum allowable NO_x emissions for marine diesel engines (IMO)

1.2 Meeting emissions regulations

The options for compliance with the IMO's new regulations according to Lloyd's Register (Farr, 2011) include the use of low sulphur fuels/distillates, HFO with a scrubber, LNG, or other alternative fuels. Lloyd's Register considers all options as feasible, but choice is dependent on commercial considerations including trading patterns and percentage of time in ECA's, cost difference and pay-back time, availability of exhaust steam cleaning technologies, and availability of LNG infrastructure. According to a ship owner survey conducted by Lloyd's Register concerning options for mitigating emissions, most owners consider LNG as the fuel most likely to provide the long term

Received date: 2013-06-15.
Accepted date: 2013-07-15.
***Corresponding author Email:** y_welaya@hotmail.com

solutions.

Germanischer Lloyd (GL) sees a large market for fuel cells to replace marine auxiliary power. The installed auxiliary power onboard seagoing vessels has a potential market of approximately 160 GW worldwide and can, in principle, be substituted by fuel cells in order to reduce air emissions. This is one of the conclusions of the market study (Barrett, 2010).

1.3 Natural gas and fuel cell opportunities in the marine field

Natural gas (made up of 70%−90% methane) is often highlighted as the cleanest fossil fuel alternative to diesel oil used for marine internal combustion engines. The cleanliness of LNG fuel is easy to appreciate when one notes it yields 100% reductions in SO_x and Particulate Matter (PM) and 92% reduction in NO_x as compared to diesel fuel. LNG also results in a 25% reduction in CO_2, a major contributor to greenhouse gas (GHG) emissions (MAN B&W, 2010).

Fuel cells (FCs) are electrochemical devices which convert the chemical fuels directly into electrical power. The Solid Oxide Fuel Cells (SOFCs) are among the high temperature fuel cells. They consist of a solid oxide electrolyte made from a ceramic such as yttria-stabilized zirconia (YSZ) which acts as a conductor of oxide ions at temperatures ranging from 600 to 1000°C. This ceramic material allows oxygen atoms to be reduced on its porous cathode surface by electrons, thus being converted into oxide ions, which are then transported through the ceramic body to a fuel-rich porous anode zone where the oxide ions can react with hydrogen or hydrogen rich gas giving up electrons to an external circuit. Therefore, the SOFC can be operated either by hydrogen or hydrocarbon reformed fuels (Welaya *et al*., 2011; Santin *et al*., 2010; Barclay, 2006). The North Western University patents of direct hydrocarbon oxidation, which deal with special catalysts and anodes, give the SOFC system the potential to use natural gas directly. This improves the opportunity to bypass the hydrogen fuel source problem (Barclay, 2006; Lisbona and Serra, 2005).

SOFC-based power plants have been investigated in many research papers and some companies, such as Wärtsilä, are trying to introduce such a system for combined heat and power (CHP) applications (Rokni, 2010a; Fontell *et al.*, 2004). Due to the high operating temperature of the SOFC stacks, hybrid SOFC and GT systems have also been studied extensively in the literature for combined heat and power (Pålsson *et al.*, 2000) and with internal biomass gasification (Proell *et al*., 2004). Characterization, quantification and optimization of hybrid SOFC–GT systems have been studied by (Subramanyan and Diwekar, 2005) and (Calise *et al*., 2006b). The dynamics and control concept of a pressurized SOFC–GT hybrid system has also been studied, such as in (Wächter *et al*., 2006). Moreover, exergy analysis of SOFC-GT hybrid systems in full load and part load operations and optimization based on exergy and thermo economics was simulated in (Calise *et al*., 2006a; 2006b).

While hybrid SOFC–GT plants have been extensively studied by many researchers, the investigations into combined SOFC and steam turbine (ST) are limited (Dunbar *et al*., 1991). Thermodynamic analysis of an integrated solid oxide fuel cell cycle with a Rankine cycle has been studied by (Rokni, 2010a; 2010b). Thermo-economic modeling and parametric study of the hybrid SOFC, gas turbine and steam turbine power plants ranging from 1.5 to 10MWe have been studied by (Arsalis, 2008). In addition, the SOFC manufacturers are trying to decrease the operating temperature of the SOFC stacks, and then the combination of the SOFC–ST hybrid system would be more economically attractive than the SOFC–GT systems (Rokni, 2010a).

In this paper a parametric study on a solid oxide fuel cell has been conducted and the effects of different parameters on the SOFC performance have been discussed. Also, the total performance of the combined solid oxide fuel cell and steam turbine is discussed.

1.4 NG and SOFC in classification societies and regulations

It is a characteristic of marine fuels and equipment to be approved by one of the members of the International Association of Classification Societies (IACS). Classification societies accepted NG as the only gas that can be used onboard. Det Norske Veritas “DNV”, China classification society, and Lloyd’s Register “LR” have regulations for natural gas driven ships to increase the safety onboard. The International Gas Code (IGC) (IMO-IGC Code, 2002; China Classification Society, 2006) provides the general arrangement; gas piping systems, fire detection alarm, gas control, monitoring systems and working pressure in the engine room.

In addition, the American Bureau of Shipping (ABS) has recently released a guide for Propulsion and Auxiliary Systems for Gas Fueled Ships (GFS). Its objectives are to provide criteria for arrangements, construction installation and operation of machinery, equipment and systems for vessels operating with natural gas as a fuel in order to minimize risks to the vessel, crew and environment (MAN B&W, 2010).

The first rules for using fuel cells were introduced by Germanischer Lloyd (GL) in 2003, together with the International gas code (IGC) development. In addition, Det Norske Veritas (DNV), Bureau Veritas (BV) and other classification societies are working hard to develop rules for using fuel cells in the marine field (Rattenbury and Fort, 2006).

2 500 kW SOFC model

As mentioned above, the solid oxide fuel cell (SOFC) is considered as one of the most promising options for marine applications for achieving IMO emission requirements. The SOFC can use natural gas directly as a fuel. For the near future, fuel cells can replace the diesel generator. The 18 MW

SOFCPP model parameters are based on a 500 kW SOFC model and a 55% fuel utilization coefficient. It consists of 36 internally reformed planar and tubular models of 500 kW connected in series and extrapolated for 18MW SOFC. The 500 kW SOFCPP model main parameters are listed in Table 1(Santin *et al*., 2010).

Table 1 500 kW SOFC model parameters

Parameter	Value
Plant net power/ kW	500
TSOFC inlet temperature/ °C	800
TSOFC outlet temperature/ °C	1000
PSOFC inlet temperature/ °C	850
PSOFC outlet temperature/ °C	950
SOFC fuel utilization coefficient/%	55
Component pressure loss/%	1–3
Component heat loss/%	1–2
Ambient pressure/ atm	1
Ambient temperature/ °C	25

Table 2 Typical values of over voltage parameters (Larminie and Dicks, 2003)

Constant	Typical Value
E_o / V	1.01
r / kΩ·cm^2	2.0×10^{-3}
A / V	0.002
m / V	1.0×10^{-4}
n / cm^2·mA^{-1}	8×10^{-3}

2.1 SOFC operational voltage

Solid oxide fuel cell voltage (V_{cell}) is the difference between cell voltage at no load, which can be called an open circuit voltage, and the specific fuel cell irreversibility or voltage drop. The following equation (1) shows the operating voltage of a fuel cell at a current density (i_{den}) (Larminie and Dicks, 2003; Maroju, 2002)

$$V_{\text{cell}} = E_o - (i_{\text{den}} \times r) - A \times \ln(i_{\text{den}}) + m \times \mathrm{e}^{(n \times i_{\text{den}})} \quad (1)$$

In this equation, E_o is the open circuit voltage, 'i_n' internal current density, 'A' is the slope of the Tafel curve, 'm' and 'n' are constants, 'r' is the specific resistance. Typical values of these constants for a SOFC are given in Table 2.

2.2 Required air, fuel and oxygen mass flow rates for the model

The required mass flow rates of hydrogen, oxygen, and air in kg/s are expressed in Eqs. (2, 3 and 4) respectively, and the value of the utilization coefficient U_f in Eq. (6) refers to the ratio of hydrogen reacted in the fuel cell (Holland and Zhu, 2007; Kumm, 1990).

The required hydrogen mass flow rate can be expressed as:

$$m_{\text{hyd.}} = \frac{1.05 \times P_{\text{FC,AC}}}{10^5 \times V_{\text{cell}}} \quad (2)$$

The required oxygen mass flow rate can be written as:

$$m_{\text{o}_2} = \frac{8.29 \times P_{\text{FC,AC}}}{10^5 \times V_{\text{cell}}} \quad (3)$$

The required air mass flow rate can be written as:

$$m_{\text{air}} = \frac{3.57 \times \lambda_{\text{air}} \times P_{\text{FC,AC}}}{10^4 \times V_{\text{cell}}} \quad (4)$$

The exit air mass flow rate can be written as:

$$m_{\text{Airexit}} = m_{\text{Air}} - m_{\text{o}_2} \quad (5)$$

The SOFC exhaust gases mass flow rate can be written as:

$$m_{\text{exhaust}} = m_{\text{Airexit}} + \left[m_{\text{fuel}} \times (1 - U_f)\right] \quad (6)$$

In addition, the hydrogen mass flow rate reacted in the fuel cell can be written as:

$$m_{\text{hyd.cons.}} = m_{\text{hyd.}} \times U_f \quad (7)$$

The hydrogen formula in Eq. (2) applies only to a hydrogen-fed fuel cell. In the case of a hydrogen/carbon monoxide mixture derived from a reformed hydrocarbon, it will be different. Eq. (8) shows the relationship between the efficiency of the fuel cell, the calorific value "CV in kJ/kg" of the fuel and the resulting fuel rate in kg/s (Sjöstedt and Chen, 2009).

$$\text{Fuel flow rate} = \frac{P_{\text{FC,AC}}}{\eta_{\text{FC}} \times \text{CV}} \quad (8)$$

3 SOFC-ST hybrid system

The main principles of combining a fuel cell and heat engines depend on the waste heat from the fuel cell. Some of the waste heat will be used to heat the reactants to the required operating temperature. The remaining heat can be used to operate a heat engine. So, the total work of this system will be the summation of the fuel cell and heat engine work as shown in Fig. 2 (Barclay, 2006; Subhash and Kevin (ed.), 2004; George *et al*., 2001).

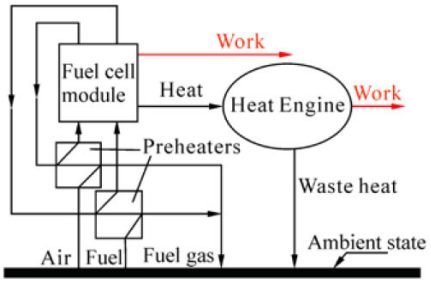

Fig. 2 Fuel cell-heat engine hybrid system

In the SOFC-ST combined cycle, the air flow to the SOFC is compressed with a steam turbine operated compressor as shown in Fig. 3. The steam turbine in the center of the diagram drives two compressors (one for the air, the other for the fuel gas) and an alternator. The air compressor is needed to drive the air through the pre-heater, the fuel cell, the afterburner, the boiler, and then out to the final heating system. The gas compressor needs to drive the fuel through the same components and so would be at a somewhat higher pressure. They would not normally compress the gases much above air pressure, and the fuel cell would operate at about only a little above ambient pressure. The natural gas is internally reformed in the fuel cell, but not all the hydrogen is consumed. The remainder is burnt in the afterburner, which raises the temperature of both gas streams. This hot gas is used in a heat exchanger type boiler to raise steam, which drives a turbine that drives the alternator (EG&G Technical Services, 2004; Ghirardo *et al*., 2011).

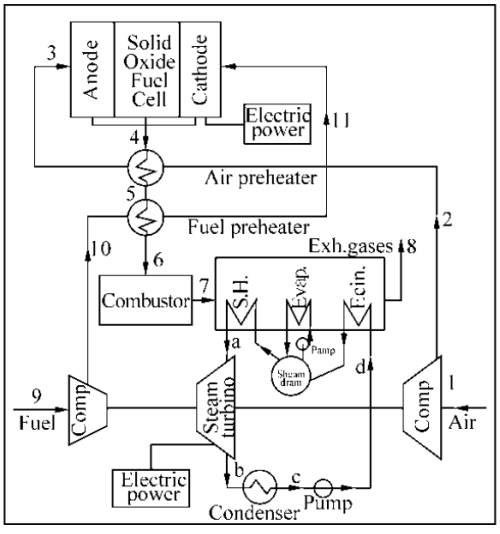

Fig. 3 SOFC-ST combined cycle schematic diagram

4 Energy formulation of components

The thermodynamic performance of each of the components introduced in the preceding section will be analyzed here. The mass and energy balance are employed under the assumption of steady flow for the entire cycle. The main stream of the working fluid, assumed as the ideal steam, at different states of the cycle is shown in Fig. 3.

A. Air and fuel compressors

The isentropic efficiency of air and fuel compressors can be defined as:

$$\eta_{\text{aircomp .}} = \frac{h_{2s} - h_1}{h_2 - h_1} \tag{9}$$

$$\eta_{\text{fuelcomp .}} = \frac{h_{10s} - h_9}{h_{10} - h_9} \tag{10}$$

Where the ideal temperature of the working fluid at the outlet of the compressor can be determined using the following equation:

$$\frac{T_{2s}}{T_1} = \left(\frac{p_2}{p_1}\right)^{(\gamma_{\text{air}}-1)/\gamma_{\text{air}}} \tag{11}$$

$$\frac{T_{10s}}{T_9} = \left(\frac{p_{10}}{p_9}\right)^{(\gamma_{\text{gas}}-1)/\gamma_{\text{gas}}} \tag{12}$$

Applying the energy balance for the system, the power required for air and fuel compressors may be obtained as follows:

$$P_{\text{aircomp .}} = \dot{m}_1 \times (h_2 - h_1) \tag{13}$$

$$P_{\text{fuelcomp .}} = \dot{m}_9 \times (h_{10} - h_9) \tag{14}$$

B. Fuel and air pre-heaters

Using the following energy balance equations for air and fuel pre-heaters, the outlet temperature of the cycle can be determined:

$$\dot{m}_2 \times C_{p_{\text{air}}} \times (T_3 - T_2) = \dot{m}_4 \times C_{p_{\text{gas}}} \times (T_4 - T_5) \tag{15}$$

$$\dot{m}_{\text{fuel}} \times C_{p_{\text{fuel}}} \times (T_{11} - T_{10}) = \dot{m}_5 \times C_{p_{\text{gas}}} \times (T_5 - T_6) \tag{16}$$

C. Solid oxide fuel cell

The fuel supplied to the system is methane (CH_4), with a lower heating value of 50 MJ/kg (Woodyard, 2004). The following electrochemical reactions expressed in Eqs. (17 to 19) occur within the anode and cathode of the fuel cell. As a comparison case, hydrogen, with a lower heating value of 120 MJ/kg (Heywood, 1988), is used for fueling the SOFC stack and combustor. Various reactions corresponding to the methane are listed below:

$$\text{Reforming: } CH_4 + H_2O \rightarrow CO + 3H_2 \tag{17}$$

$$\text{Shift gas reaction: } CO + H_2O \rightarrow CO_2 + H_2 \tag{18}$$

$$\text{Electrochemical: } H_2 + 0.5O_2 \rightarrow H_2O \tag{19}$$

The degree to which an anode supports direct oxidation will then impact the degree of pre-reforming of the fuel that is required, which in turn typically impacts the balance of plant complexity and cost (Subhash and Kevin (ed.), 2004; EG&G Technical Services, 2004). The net cell reaction is thus written as:

$$CH_{4,\text{anode}} + 2O_{2,\text{cathode}} \Leftrightarrow 2H_2O_{,\text{anode}} + CO_{2,\text{anode}} \tag{20}$$

And the net cell reaction for hydrogen as a fuel is as follows:

$$H_{2,\text{anode}} + 0.5O_{2,\text{cathode}} \Leftrightarrow H_2O_{,\text{anode}} \tag{21}$$

The maximum electrical work obtainable in a fuel cell operating at a constant temperature and pressure is given by the change in Gibbs free energy (Δg_f) of the electrochemical reaction. If all the energy from the fuel was transformed into electrical energy, then the reversible open circuit voltage, E_o, would be given by (Larminie and Dicks, 2003; Raja *et al*., 2006):

$$E_o = \frac{-\Delta g_f}{z \times F} \tag{22}$$

In addition, the efficiency of the fuel cell can be expressed as:

$$\eta_{FC} = U_f \frac{V_{cell}}{E_o} \tag{23}$$

The difference between the actual cell voltage and the open cell voltage represents the energy converted into heat energy. So, the SOFC heating power in kW can be calculated from Eq. (24) (Sjöstedt and Chen, 2009):

$$P_{heat} = P_{FC,AC} \times \left(\frac{1.25}{V_{cell}} - 1\right) \tag{24}$$

The efficiency limit for heat engines such as steam and steam turbines can be calculated using the Carnot efficiency limit which shows their maximum efficiency, but fuel cells are not subject to the Carnot efficiency limit. It is commonly supposed that if there were no 'irreversibilities' then the efficiency could be 100%. Fig.4 shows the Carnot efficiency for heat engines, fuel cell efficiency limit, and fuel cell-heat engines combined cycle maximum efficiency (Larminie and Dicks, 2003).

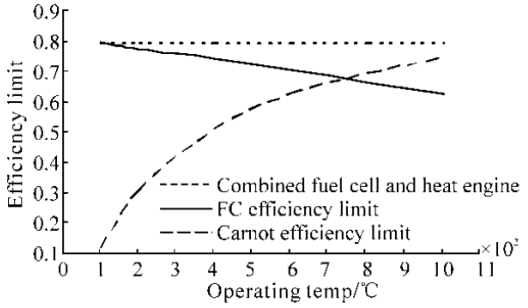

Fig. 4 Efficiency limit for the fuel cell, heat engines, and combined systems

The mass balance for the SOFC system gives:

$$\dot{m}_3 + \dot{m}_{fuel} = \dot{m}_4 + \dot{m}_{fuel} \times (1 - U_f) \tag{25}$$

The last term on the right hand side of the above equation represents the non-reacted mass flow rate that leaves the fuel cell downstream of the products. Applying the first law of thermodynamics to the SOFC and assuming an adiabatic process,

$$\begin{aligned}&(\dot{m}_3 \times h_3) + (\dot{m}_{fuel} \times U_f \times CV) + \\ &(\dot{m}_{fuel} \times (1 - U_f) \times h_{fuel,in} = \\ &\dot{W}_{FC,DC} + (\dot{m}_4 \times h_4)\end{aligned} \tag{26}$$

D. Combustor

The working fluid of the cycle, with products from the fuel cell, is further heated within the combustor. Considering that a non-reacted flow of fuel from the SOFC is burnt in the combustor and applying the mass balance for combustor gives:

$$\dot{m}_6 + \dot{m}_{fuel} \times (1 - U_f) = \dot{m}_7 \tag{27}$$

Applying the first law of thermodynamics for the combustor we get:

$$\begin{aligned}&(\dot{m}_6 \times h_6) + (\dot{m}_{fuel} \times (1 - U_f) \times CV \times \eta_{comb.}) = \\ &\dot{m}_7 \times h_7\end{aligned} \tag{28}$$

where, $\eta_{comb.}$ represents the efficiency of the combustor.

E. Exhaust gas boiler

Typical temperature profiles of exhaust gas and steam/water in the exhaust gas boiler are shown in Fig. 5. The exhaust gas enters the super heater at T_{go} where the saturated steam is superheated to high temperature T_{SH}. The exhaust gas then enters the evaporator at T_{g1} where a mixture of saturated water and saturated steam exists. The exhaust gas leaves the evaporator at T_{g2} and the pinch point (TPP) means the temperature difference between T_{g2} and the saturated temperature $T_{sat.}$ The exhaust gas is discharged to the environment at T_{g3}.

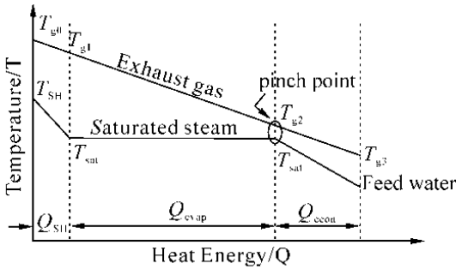

Fig. 5 T-Q diagram for the exhaust gas boiler (EGB)

The governing equations for the heat available in the gas down to the pinch point (T_{go} to T_{g2}), and the corresponding heat absorbed by the superheated and saturated steam are presented below:

$$Q^{gas}_{SH+Evap.} = \dot{m}_{gas} \times C_{p_{gas}} \times (T_{go} - T_{g2}) \tag{29}$$

$$Q^{steam}_{SH+Evap.} = \dot{m}_{steam} \times (h_{superheated} - h_f) \tag{30}$$

Substituting this heat value into the steam side equation to solve directly for the steam mass flow rate is shown in the following equation:

$$Q^{gas}_{SH+Evap.} = Q^{steam}_{SH+Evap.} \tag{31}$$

Knowing the water/steam mass flow rate, the EGB heat duty can be calculated using the following equation:

$$Q^{steam}_{Total} = \dot{m}_{steam} \times (h_{superheated} - h_{feedwater}) \tag{32}$$

The steam temperature leaving the EGB (T_{g3}) is now easily calculated, because the total heat transferred to the steam is equivalent to that lost by the gas stream:

$$Q_{\text{Total}}^{\text{gas}} = \dot{m}_{\text{gas}} \times C_{\text{p}_{\text{gas}}} \times \left(T_{\text{go}} - T_{\text{g3}}\right) \quad (33)$$

F. Steam turbine

Knowing the EGB heat duty, the superheated steam enthalpy (h_a) can be calculated using the following equation:

$$Q_{\text{Total}}^{\text{gas}} = \dot{m}_{\text{steam}} \times (h_a - h_d) \quad (34)$$

The outlet enthalpy of the steam turbine, h_b, can be determined from the definition of isentropic efficiency of the turbine,

$$\eta_{\text{st,isen.}} = \frac{h_a - h_b}{h_a - h_{bs}} \quad (35)$$

The required power for the natural gas and air compressor is provided by steam turbine power as shown in Fig.3. So, the steam turbine net power can be calculated using the following equation:

$$P_{\text{stnet}} = P_{\text{st}} - P_{\text{fuelcomp.}} - P_{\text{aircomp.}} \quad (36)$$

where,

$$P_{\text{st}} = \dot{m}_{\text{steam}} \times [(h_a - h_b) - (h_d - h_c)] \quad (37)$$

G. Overall balance equations for the integrated cycle

The integrated steam turbine power plant with the SOFC in Fig.3 may be analyzed as a lumped control volume. In the following, mass balance as well as the first and second laws of thermodynamics can be derived from the above mentioned control volume.

The mass balance for the total system can be written as:

$$\dot{m}_1 + \dot{m}_{\text{fuel}} = \dot{m}_8 \quad (38)$$

$$\dot{m}_1 = \dot{m}_2 = \dot{m}_3 \quad (39)$$

$$\dot{m}_7 = \dot{m}_8 \quad (40)$$

Overall energy balance can be expressed as:

$$\begin{aligned}&(\dot{m}_1 \times h_1) + (\dot{m}_{\text{fuel}} \times U_f \times \text{CV}) + \\ &(\dot{m}_{\text{fuel}} \times (1 - U_f) \times \text{CV} \times \eta_{\text{comb.}}) = \\ &(\dot{m}_8 \times h_8) + \dot{W}_{\text{FC,DC}} + P_{\text{stnet}}\end{aligned} \quad (41)$$

The combined cycle efficiency can be expressed as:

$$\eta_{\text{combined}} = \frac{P_{\text{FC,AC}} + P_{\text{stnet,elec.}}}{\dot{m}_{\text{fuel}} \times \text{CV}} \quad (42)$$

where,

$$P_{\text{stnet,elec.}} = P_{\text{stnet}} \times \eta_{\text{gen.}} \quad (43)$$

The steam turbine cycle efficiency can be expressed as:

$$\eta_{\text{st}} = \frac{P_{\text{stnet,elec.}}}{\dot{m}_{\text{fuel}} \times \text{CV}} \quad (44)$$

5 Results and discussion

The temperature difference (Δt) between the exhaust gas temperature at the SOFC exit and the live steam temperature in the waste heat boiler in a combined system was assumed to be equal to Δt = 50°C. The "pinch point" value recommended by MAN for boilers is equal to Δt = 10 °C. The calculations were preformed assuming that the feed water temperature is within $t_{\text{feedwater}}$(10–50)°C. It was also assumed that the exhaust gas temperature at the boiler exit should be higher than that of the feed water temperature (Olszewskin, 2011). The assumed super-heated steam and condenser pressures are 9.0 and 0.04 bars respectively with an evaporator drum pressure of 11.5 bars (EG&G Technical Services, 2004; Olszewski, 2011). Moreover, the use of materials revealing extended resistance to acid corrosion is recommended.

In addition, this study assumes a 55% utilization coefficient of fuel in the cells. Table 3 summarizes the data of the different auxiliary system components utilized in the combined SOFC-ST plant (Larminie and Dicks, 2003; EG&G Technical Services, 2004).

Table 3 Auxiliary system component data for the SOFC-ST plant

Component	Parameter	Value
Air compressor	Isentropic efficiency ($\eta_{\text{aircomp.}}$)	85%
Fuel compressor	Isentropicefficiency ($\eta_{\text{fuelcomp.}}$)	81%
Steam turbine	Isentropicefficiency ($\eta_{\text{st,isen.}}$)	88%
Combustor	Combustion efficiency ($\eta_{\text{comb.}}$)	98%
AC generator	Electric efficiency (η_{gen})	90%
DC/AC Converter	Conversion efficiency	95%
SOFC stack	Pressure loss	3%
Combustor	Pressure loss	2%

5.1 SOFC power plant results

The performance of a solid oxide fuel cell stack is usually described by the polarization curve, which relates the cell voltage to its current density. This polarization curve is affected by the losses of the fuel cell.

Fig. 6 shows the polarization curve of the SOFC case study. As the cell current increases from zero, there will be a drop of the output voltage of the SOFC. This drop of the cell voltage is due to activation voltage loss. Then, almost a linear decrease of the cell voltage is seen as the cell current increases beyond certain values, as shown in Fig. 6, which is a result of the ohmic loss. Finally, the cell voltage drops sharply to zero as the load current approaches the maximum current density that can be generated by the fuel cell. The sharp voltage drop is the effect of the concentration loss in the fuel cell.

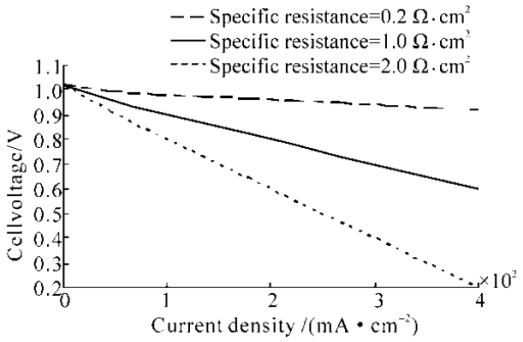

Fig.6 SOFC voltage at different specific resistance

Prediction of the maximum available voltage from the cell process involves evaluation of energy differences between the initial states of reactants in the fuel cell process. Open circuit voltage of the SOFC plays an important role in the cell performance. Fig.7 shows the effects of changing the open circuit voltage on SOFC operational voltage and efficiency. As the open circuit voltage increases, the SOFC operational voltage will be increased which improves the cell efficiency.

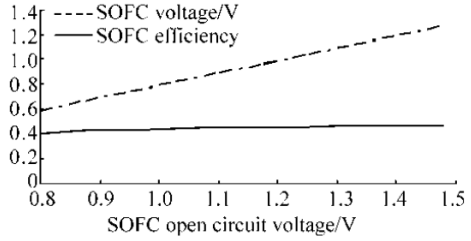

Fig. 7 SOFC operational voltage and efficiency at different open cell voltages

The value of fuel mass flow depends on the fuel utilization coefficient and cell voltage for the SOFC. Figs.8 and 9 show the effects of fuel cell voltage on the consumption of hydrogen and natural gas for different SOFC power plants. The higher voltage of the SOFC will correspond to higher SOFC efficiency. So, the hydrogen and natural gas mass flow rates decrease as the SOFC voltage increases.

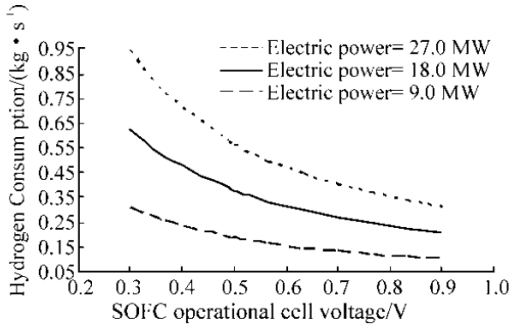

Fig. 8 Hydrogen fuel consumption for SOFC at different electric powers

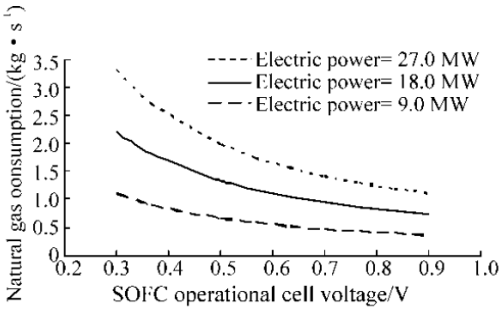

Fig. 9 Natural gas fuel consumption for SOFC at different electric powers

An essential aspect of SOFC design and application is the heat produced by the electrochemical reaction. Heat is inevitably generated in the SOFC by ohmic losses, electrode over potentials, etc. These losses are present in all designs and cannot be eliminated but must be integrated into a heat management system. Indeed, the heat is necessary to maintain the operating temperature of the cells. The benefit of the SOFC over competing fuel cells is the higher temperature of the exhaust heat which makes its control and utilization simple and economical. Fig.10 shows the heating power losses from the SOFC with cell voltage at different ranges of output power.

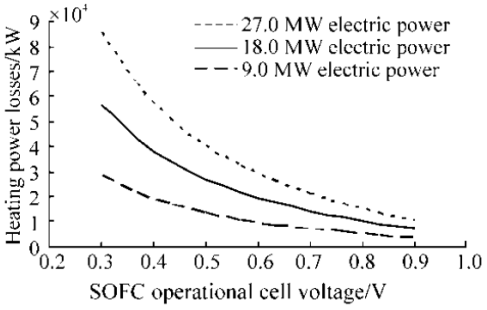

Fig. 10 Heat losses from SOFC at different electric Powers

5.2 SOFC-ST power plant results

One of the great benefits of the SOFC is that it can utilize a wide range of fuels. The fastest reaction at the nickel anode is that of hydrogen. But other fuels can also react directly on the anode, depending on catalyst composition. In this study two types of fuel are included, hydrogen and natural steam. Four layouts have been studied. They include the tubular SOFC (TSOFC), and the planar SOFC (PSOFC) using natural gas internal reforming and pure hydrogen fuels.

The selected operating point for the combined SOFC-ST cycle is at cell output current density of 100 mA/cm^2, cell voltage of 0.8 volts, and a fuel utilization coefficient of 55% (Rokni, 2010a; 2010b; Larminie and Dicks, 2003). At this operating point the mass flow of fuel consumption is 0.236 kg/s and 0.826 kg/s for hydrogen and natural gas respectively. The inlet fuel temperature to the SOFC is assumed to be 100^{o}C.

In addition, the mass flow rate of the air used for the SOFC-ST cycle depends on the type of fuel used. Air consumption for hydrogen fuel is 20.06 kg/s calculated using Eq. (4), which is nearly half the assumed value if natural gas fuel is used (Larminie and Dicks, 2003).

Also, the values of the inlet and outlet temperatures of the SOFC depend on the type of SOFC modules. For the TSOFC the temperatures are 1073k and 1273k for the inlet and outlet flows respectively. The PSOFC has a higher inlet temperature of 1123k and a lower outlet temperature of 1223k as compared with the TSOFC modules.

Fig.11 shows the effects of superheated steam pressure on steam cycle efficiency. The cases include planar and tubular SOFCs operated with natural gas incorporating internal reforming at the anode or hydrogen. The tubular SOFC has a higher efficiency than the planar SOFC.

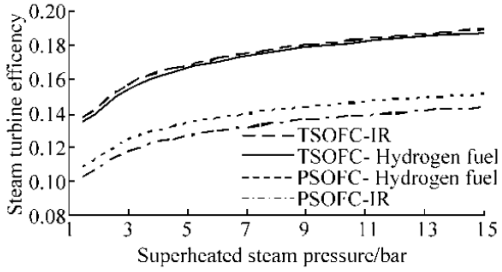

Fig. 11 Comparison of steam turbine efficiency for various SOFC hybrid systems at different superheated steam pressures

The combined cycle efficiency is affected by the type of fuel used. Hydrogen fuel has the highest hybrid efficiency over different superheated steam pressures as shown in Fig. 12.

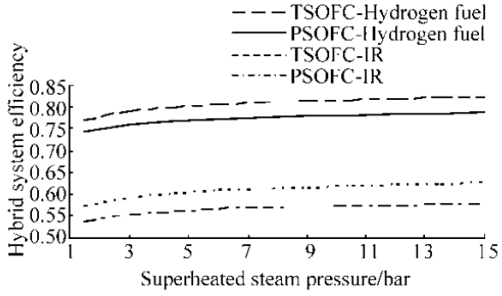

Fig.12 Comparison of hybrid system efficiency for various SOFC hybrid systems at different superheated steam pressures

The mass flow rate of air used plays an important role in determining the efficiency of the SOFC-ST hybrid cycle. In addition, steam cycle efficiency decreases as inlet flow rate increases as shown in Fig.13. The steam cycle associated with the TSOFC has higher efficiency at different inlet air flows than the PSOFC steam cycle. So, the TSOFC hybrid system with internal reforming achieves higher efficiency than the PSOFC hybrid system.

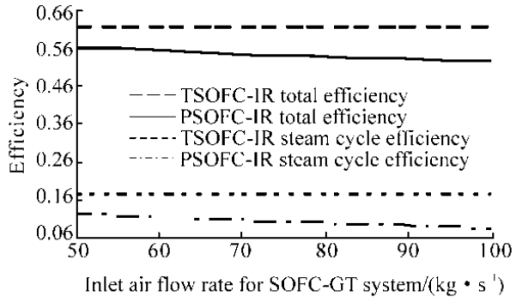

Fig.13 Hybrid and steam turbine efficiencies variation with inlet air mass flows for hybrid system

The fuel utilization coefficient not only affects the SOFC performance, but also affects the SOFC-ST hybrid system efficiency. At higher fuel utilization coefficients, the hybrid efficiency will be increased for both the TSOFC and the PSOFC as shown in Fig.14.

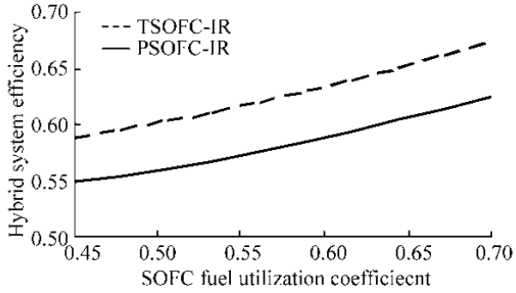

Fig. 14 Effects of the fuel utilization coefficient on hybrid system efficiency for TSOFC and PSOFC

The SOFC voltage determines the main characteristics of the cell. It also affects both the total hybrid system power and output power from the low pressure power turbine and required power for compressor. Fig.15 shows the variation in ST efficiency and hybrid system efficiency with natural gas internally reformed SOFC voltage.

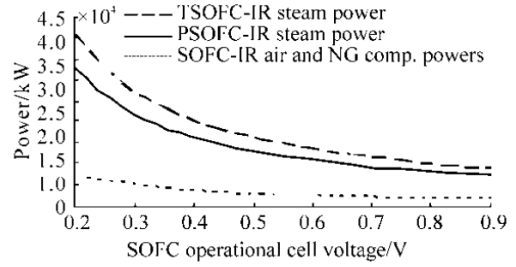

Fig.15 Auxiliary system power variation with SOFC operational voltage for hybrid system

In addition, the variation of the SOFC voltage affects the total hybrid system efficiency as the efficiency of the SOFC will be changed. On the other hand, the SOFC voltage variations have almost no effect on the steam cycle efficiency as shown in Fig.16. The total hybrid SOFC-ST efficiency increases as the cell voltage increases.

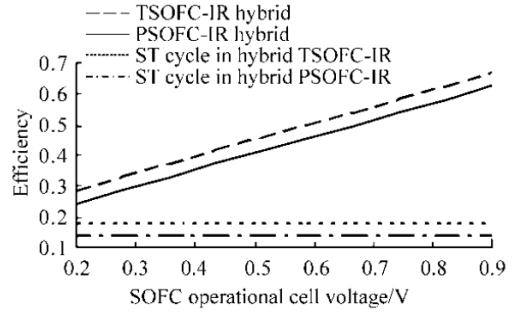

Fig.16 Hybrid and steam turbine efficiencies variation with SOFC operational voltage for hybrid system

The variation of the output current density of the SOFC changes the performance of both systems of the SOFC and the SOFC-ST. As the current density increases, the total hybrid system efficiency increases. On the other hand, current density has almost no effect on steam turbine efficiency like cell voltage variation. It only affects SOFC and hybrid efficiency. At high current density, SOFC voltage reduces greatly and this reduction in voltage is converted into heat energy. So, at high current density, steam turbine output power is high for the combined tubular and planar SOFC as shown in Fig.17.

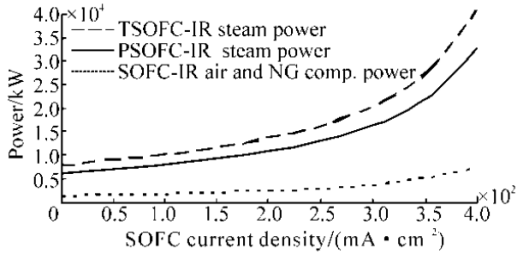

Fig.17 Steam cycle required and output powers for compressor and power turbine at different SOFC output current densities

6 Conclusion

The thermodynamic analysis of the natural gas and hydrogen-fuelled SOFC was presented as a proposed solution to achieve high efficiency and satisfy the requirements of international regulations. Both the TSOFC and PSOFC are integrated with the steam turbine cycle to make use of the waste heat of the SOFC. Four layouts were studied, combining two SOFC modules with steam turbines operated either by natural gas through internal reforming or hydrogen. Thermodynamic considerations are used to understand the process of energy conversion in SOFCs. The reversible work of a fuel cell is defined by the free or Gibbs enthalpy of the reaction. The mass flow of the consumed fuel is proportional to the electric current and the reversible work is proportional to the reversible voltage.

The parameters, which affect fuel cell performance, include the cell voltage, open cell voltage, fuel cell efficiency, and fuel utilization coefficient. The actual SOFC cell voltage is 0.801 volt at 100 mA/cm2 output current density with cell efficiency of 43.62%, and the open cell voltage is 1.01 volt. These values affect the hybrid efficiency and the performance of the SOFC. The proposed model of the 18 MW SOFC power plant shows that the percentage of power lost in heating for the fuel cell power plant is 10.089MW with a percentage of 24.4 % of the total input for the SOFC at 100 mA/cm^2 output current density.

The combination of a SOFC with a ST has a high electric efficiency. The main parameters which affect the SOFC-ST power plant are superheated steam pressure, inlet air mass flow rate, SOFC fuel utilization coefficient, cell voltage, and cell output current density. The SOFC-ST system is very suitable for high-efficiency power generation. At the operating point of 100 mA/cm^2, the total hybrid TSOFC-IR-ST efficiency is 59.38%. So, the combined SOFC-ST exceeds that of the SOFC plant by 15.76% with respect to thermal efficiency, and in addition, produces less emission. Finally, TSOFCs have a higher output temperature of exhaust gas and total thermal efficiency than PSOFCs.

Nomenclature

C_{pair}	Air specific heat at constant pressure, kJ/kg·K
$C_{\text{p fuel}}$	Fuel specific heat at constant pressure, kJ/kg·K
$C_{\text{pgas.}}$	Gas specific heat at constant pressure, kJ/kg·K
CV	Fuel calorific value, kJ/kg
E_o	Open circuit voltage, volt
F	Faraday's constant Coulomb/mole
h	Enthalpy, kJ⁄kg.
$h_{\text{feedwater}}$	Feed water to EGB enthalpy, kJ/kg
$h_{\text{superheated}}$	Superheated steam enthalpy, kJ/kg
$\text{h}_{\text{fuel,in}}$	Inlet fuel enthalpy, kJ/kg
i_{den}	Current density, mA⁄cm^2.
$\dot{m}$	Mass flow rate, kg/s
m_{Air}	Required Air mass flow rate, kg/s
m_{Airexit}	Exit Air mass flow rate of SOFC, kg/s
m_{exhaust}	Exhaust gases mass flow rate of SOFC, kg/s
$m_{\text{hyd.}}$	Required hydrogen mass flow rate, kg/s
$m_{\text{hyd.cons.}}$	Hydrogen mass flow rate reacted in fuel cell, kg/s
m_{o_2}	Required oxygen mass flow rate, kg/s
m_{steam}	Steam mass flow rate, kg/s
$\dot{m}_{\text{fuel}}$	Total input fuel flow rate, kg/s
p	Pressure, bar
$P_{\text{FC,Ac}}$	AC power output of the cell stack, kW
P_{st}	Steam cycle output power, kW
P_{stnet}	Net output power of steam cycle, kW
$P_{\text{stnet,elec.}}$	Net electric output power of steam cycle, kW
P_{heat}	Heating loss power, kW
$P_{\text{aircomp·}}$	Air compressor required power, kW
$P_{\text{fuelcomp.}}$	Fuel compressor required power, kW
$Q^{\text{gas}}_{\text{SH+Evap.}}$	Heat absorbed by the superheated and saturated exhaust gas streams, kW
$Q^{\text{steam}}_{\text{SH+Evap.}}$	Heat absorbed by the superheated and saturated steam streams, kW

$Q_{\text{Total}}^{\text{gas}}$	Total heat lost by the exhaust gas stream, kW
$Q_{\text{Total}}^{\text{steam}}$	Exhaust gas boiler heat duty, kW
T	Temperature, K
U_f	Fuel utilization coefficient
V_{cell}	Fuel cell voltage, volts
$\dot{W}_{\text{FC,DC}}$	DC power output of the cell stack, kW
z	Number of electrons transferred for each molecule of fuel

Greek letters

Δg_f	Change in Gibbs free energy of an electrochemical reaction, kJ /mole
γ_{air}	Air specific heats ratio
γ_{gas}	Gas specific heats ratio
η	Efficiency
$\eta_{\text{aircomp.}}$	Air compressor isentropic efficiency
$\eta_{\text{comb.}}$	Combustor efficiency
η_{combined}	Combined (hybrid) efficiency
η_{FC}	Fuel cell efficiency
$\eta_{\text{fuelcomp.}}$	Fuel compressor isentropic efficiency
$\eta_{\text{gen.}}$	Generator efficiency
η_{st}	Steam turbine cycle efficiency
$\eta_{\text{st,isen.}}$	Steam turbine isentropic efficiency
λ_{Air}	Stoichiometric ratio of air

Abbreviations

CO_2	Carbon dioxide
CO	Carbon monoxide
ECA	Emission control area
EGB	Exhaust gas boiler
H_2	Hydrogen
H_2O	Water vapor
HFO	Heavy fuel oil
IMO	International Maritime Organization
LNG	Liquefied natural gas
MARPOL	International marine pollution prevention convention
NG	Natural gas
NO_x	Nitrogen oxides emissions
CH_4	Methane
O_2	Oxygen gas
PM	Particulate Matter
PSOFC	Planar SOFC
PSOFC-IR	Planar SOFC-NG Internal reforming
SOFC	Solid oxide fuel cell
SOFC-ST	Solid oxide fuel cell combined cycle
SOFCPP	Solid oxide fuel cell power plant
SO_x	Sulfur oxide emissions
ST	Steam turbine
TSOFC	Tubular SOFC
TSOFC-IR	Tubular SOFC-NG Internal reforming

References

Arsalis A (2008). Thermo economic modeling and parametric study of hybrid SOFC gas turbine steam turbine power plants ranging from 1.5 to 10MWe. *Journal of Power Sources*, **181**, 313–326.

Barclay JF (2006). *Fuel cells, engines and hydrogen an exergy approach.* john wiley & sons ltd, the atrium, southern gate, chichester, West Sussex PO19 8SQ, England: 13 978-0-470-01904-7.

Barrett S (2010). GL sees large market for fuel cells to replace marine auxiliary power. *Fuel Cells Bulletin*, German National Innovation Program for Hydrogen and Fuel Cell Technology: www.now-gmbh.de/index.

Calise F, d'Accadia MD, Palombo A, Vanoli L (2006a). Simulation and exergy analysis of a hybrid solid oxide fuel cell (SOFC) and gas turbine system. *Energy*, **31**(15), 3278–99.

Calise F, d'Accadia MD, Vanoli L, Von Spakovsky MR (2006b). Single level optimization of a hybrid SOFC–GT power plant. *Journal of Power Sources*, **159**(2), 1169–1185.

China Classification Society (2006). Rules for construction and equipment of ships carrying liquefied gases in bulk. Beijing.

Corbett JJ, Winebrake JJ, Green EH, Kasibhatla P, Eyring V, Lauer A (2007). Mortality from ship emissions: a global assessment. *Environmental Science and Technology*, **41**(24), 8512–8518.

Dunbar WR, Lior N, Gaggioli RA (1991). Combining fuel cells with fuel-fired power plants for improved exergy efficiency. *Journal of Energy*, **16**(10), 1259–74.

EG&G Technical Services, Inc. (2004). *Fuel Cell Handbook*. Seventh Edition, National Technical Information Service, U. S. Department of Commerce.

Farr J (2011). LNG as a Fuel for Marine Applications.Lloyd's Register. Middle East and Africa Advisory Technical Committee.

Figari M, D'Amico M, Gaggero P (2011). Evaluation of ship efficiency indexes. *14th Conference of the International Maritime Association of the Mediterranean (IMAM)*, Genoa, 621-627.

Fontell E, Kivisaari T, Christiansen N, Hansen J, Pålsson JB (2004). Conceptional study of a 250 kW planar SOFC system for CHP application. *Journal of Power Sources*, **131**, 49–56.

George RA, *et al.* (2001). Single Module Pressurized Fuel Cell Turbine Generator System. US Patent (pending), WO 01/06589 A1.

Ghirardo F, *et al.* (2011). Heat recovery options for onboard fuel cell systems. *Journal of Hydrogen Energy*, **36**, 8134-8142.

Greensmith G (2010). The Legislative Landscape, Lloyd's Register. Middle East and Africa Advisory Technical Committee: www.cdlive.lr.org.

Heywood JBL (1988). *Internal Combustion Engines*. McGraw-Hill, Inc, 0-07-028637-X, 70-80.

Holland BJ, Zhu JG (2007). Design of A 500 W PEM fuel cell test system. Faculty of Engineering, University of Technology, Sydney, PO Box 123, Broadway, NSW.

IMO-IGC Code (2002). International gas code for construction and equipment of ships carrying liquefied gases in bulk.

Kumm WH (1990). Marine and naval applications of fuel cells for propulsion: the process selection. *Journal of Power Sources*, **29**, 20-25.

Larminie J, Dicks A (2003). *Fuel cell systems explained*. 2nd Edition, England: John Wiley & Sons Ltd. 0-470-84857-X, 60-91.

LisbonaPU, Serra JL (2005). High-temperature fuel cells for fresh water production. *Journal of Desalination*, **182**, 471–482.

MAN B&W (2010). Exhaust Gas Emission Control Today and Tomorrow, Application on MAN B&W Two-stroke Marine Diesel Engines. MAN Diesel, Copenhagen, Denmark.

Maroju P (2002). *Modeling of a fuel cell*. Master of Science thesis, Texas Tech University, 36-40.

Olszewski W (2011). Possible use of combined Diesel engine and steam turbine systems in ship power plants, *Scientific Journals*, **28**, 88–94.

Pålsson J, Selimovic A, Sjunnesson L (2000). Combined solid oxide fuel cell and gas turbine system for efficient power and heat generation. *Journal of Power Sources*, **86**, 442–448.

Proell T, Rauch R, Aichering C, Hofbauer H (2004). Coupling of biomass steam gasification and an SOFC–GT hybrid system for highly efficient electricity generation. *ASME Turbo Expo Proceeding*, GT2004-53900, 103–109.

Raja AK, Srivastava AP, Dwivedi M (2006). *Power plant engineering*. New Age International (P) Ltd, 20-35.

Rattenbury N, Fort E (2006). Development of requirements for fuel cells in the marine environment performance and prescription. Lloyd's Register Technical Papers.

Rokni M (2010a). Thermodynamic analysis of an integrated solid oxide fuel cell cycle with a rankine cycle. *Energy Conversion and Management*, **51**, 2724–2732.

Rokni M (2010b). Plant characteristics of an integrated solid oxide fuel cell cycle and a steam cycle. *Energy*, **35**, 4691-4699.

Santin M, Traverso A, Magistri L, Massardo A (2010). Thermo economic analysis of SOFC-GT hybrid systems fed by liquid fuels. *Journal of Energy*, **35**, 1077–1083.

Sjöstedt CJ, Chen DJ (2009). Virtual component testing for pem fuel cell systems: an efficient, high-quality and safe approach for suppliers and OEM´s. *3rd European PEFC Forum*, Session B09.

Subhash CS, and Kevin K (ed.) (2004). *High temperature solid oxide fuel cells: fundamentals, design and applications*. Elsevier Advanced Technology, The Boulevard, Langford Lane, Kidlington Oxford OX5 lGB, UK, 1856173879.

Subramanyan K, Diwekar UM (2005). Characterization and quantification of uncertainty in solid oxide fuel cell hybrid power plants. *Journal of Power Sources*, **142**, 103–106.

Wächter C, Lunderstädt R, Joos F (2006). Dynamic model of a pressurized SOFC–GT hybrid power plant for the development of control concept. *Journal of Fuel Cell Science and Technology*, **3**(3), 271–9.

Welaya YMA, El Gohary MM, Ammar NR (2011). A comparison between fuel cells and other alternatives for marine electric power generation. *International Journal of Naval Architecture and Ocean Engineering (JNAOE)*, **3**, 141-149.

Woodyard D (2004). *Pounder's marine diesel engines and gas turbines*. 8th edition, Elsevier, 0 7506 5846 0, 25-35.

Author biographies

Yousri M. A. Welaya is an emeritus professor at the Department of Naval Architecture and Marine Engineering, Alexandria University. Current research work includes the dynamic behavior of damaged semi-submersibles, environmental loading on offshore structures and energy management options in marine power plants.

M. Mosleh is a professor at the Department of Naval Architecture and Marine Engineering, Alexandria University. Current research work includes automatic control applications in the marine field, advanced marine diesel engines, marine power plants and marine engineering.

Nader R. Ammar is a PhD candidate with the Faculty of Engineering, Alexandria University. He is a teaching assistant at The Department of Naval Architecture and Marine Engineering. His current research interests include fuel cell applications in the marine field, renewable energy and modern marine power plants.